

## Article

# Tribological Performance of Steel/W-DLC and W-DLC/W-DLC in a Solid–Liquid Lubrication System Additivated with Ultrathin MoS<sub>2</sub> Nanosheets

Meirong Yi <sup>1,2</sup>, Taoping Wang <sup>1,2</sup>, Zizheng Liu <sup>1,2</sup>, Jin Lei <sup>1,2</sup>, Jiaxun Qiu <sup>1,2</sup> and Wenhui Xu <sup>1,2,\*</sup>

<sup>1</sup> School of Advanced Manufacture, Nanchang University, Nanchang 330031, China; yimr18@ncu.edu.cn (M.Y.); 18779475197@163.com (T.W.); 15079551992@163.com (Z.L.); 15946993985@163.com (J.L.); 17746676641@163.com (J.Q.)

<sup>2</sup> Key Laboratory of Tribology, Nanchang University, Nanchang 330031, China

\* Correspondence: flipreverse@126.com

**Abstract:** In this paper, MoS<sub>2</sub> nanosheets with an ultrathin structure were fabricated using a solvothermal method and further added into PAO oil, which was further combined with W-DLC coating to constitute a solid–liquid lubricating state. The influences of MoS<sub>2</sub> concentration, applied load and counter surfaces on the lubricating of the solid–liquid hybrid lubricating system were explored through a ball-on-disk tribometer. The friction results indicated that the steel/W-DLC and W-DLC/W-DLC tribopairs lubricated with ultrathin MoS<sub>2</sub> possessed better friction reduction and wear resistance behaviors in comparison to pure PAO oil. However, compared to the steel/steel couple case, the prepared MoS<sub>2</sub> nanosheets exhibited a more efficient lubricating effect for the W-DLC/W-DLC couple. The beneficial boundary lubricating impact of MoS<sub>2</sub> nanosheets on self-mated W-DLC coated rubbing surfaces could be attributed to the tribochemical reaction between MoS<sub>2</sub> and doping W element in DLC, resulting in a formation of a thin tribofilm at both counterparts. Meanwhile, the extent of graphitization of W-DLC film induced by friction was alleviated because of the lubrication and protection from the formation of MoS<sub>2</sub>-based tribofilm at both counterparts.

**Keywords:** W-DLC coating; ultrathin MoS<sub>2</sub> nanosheets; lubricating additive; solid–liquid composite lubrication; friction; wear



**Citation:** Yi, M.; Wang, T.; Liu, Z.; Lei, J.; Qiu, J.; Xu, W. Tribological Performance of Steel/W-DLC and W-DLC/W-DLC in a Solid–Liquid Lubrication System Additivated with Ultrathin MoS<sub>2</sub> Nanosheets. *Lubricants* **2023**, *11*, 433. <https://doi.org/10.3390/lubricants11100433>

Received: 22 August 2023

Revised: 28 September 2023

Accepted: 28 September 2023

Published: 7 October 2023



**Copyright:** © 2023 by the authors. Licensee MDPI, Basel, Switzerland. This article is an open access article distributed under the terms and conditions of the Creative Commons Attribution (CC BY) license (<https://creativecommons.org/licenses/by/4.0/>).

## 1. Introduction

Solid–liquid composite lubricating systems have always been an important research focus, because they can largely offer excellent tribological property and undertake serious operating environments [1–3]. Diamond-like carbon (DLC) coating is a solid lubrication material with outstanding worn resistance, low friction coefficient and high hardness, which makes it suitable for protective films for multifarious mechanical parts [4,5]. Since traditional lubricant additives have been developed and customized for lubricating metallic surfaces, there was no consistent opinion concerning the lubrication efficacy of lubricating additives on the DLC coated surfaces. Tannous et al. [6] have compared the tribological properties of IF-MoS<sub>2</sub> in different tribopairs of steel/steel, alumina/alumina and DLC/DLC, respectively. They have suggested that the friction reduction behavior of MoS<sub>2</sub> particles was only achieved for steel surfaces, with no effect for other friction pairs of alumina or DLC. Meanwhile, they have also pointed out that a MoS<sub>2</sub>-based tribofilm was merely found on the rubbed ferrous surfaces due to the occurrence of a tribochemical reaction between MoS<sub>2</sub> and the iron-based surfaces. However, Kalin et al. [7] have obtained a positive lubrication effect for the self-mated DLC-coated surfaces through utilizing MoS<sub>2</sub> nanotubes as oil additives. They have attributed this to the fact that MoS<sub>2</sub> flakes physically attached to the DLC-coated surfaces, which contributed to a formation of thin tribofilm at both counterparts. It can be seen that some conflicting opinions on the lubrication efficacy

of DLC-coated friction surfaces lubricated with nanoparticle additivated oil. Accordingly, more work is required for the successful application of DLC coating under the liquid-lubricated case.

In recent decades, a huge amount of research has been directed to employing nanoparticles as lubricant additives, including carbon [8], metals [9], sulfides [10], hydroxides [11], borates [12], etc. Especially, MoS<sub>2</sub> nanoparticles have obtained impressing attention arising from their particular layered structure [13]. The tribological response of MoS<sub>2</sub> nanoparticles as lubricant additives for metal friction pairs has been extensively studied in previous research. As is widely acknowledged, MoS<sub>2</sub> nanosheets are excellent solid lubricant additives for steel-based friction surfaces [14,15]. A latest tendency in the preparation of MoS<sub>2</sub> lubricant additives is to synthesize MoS<sub>2</sub> nanosheets with ultrathin structure to facilitate their entrance into the rubbing interfaces and accordingly optimizing the lubrication performance of oils. For example, Yi et al. [16] recently reported that ultrathin MoS<sub>2</sub> nanosheets could better enhance the tribological behavior of oils, as they were penetrated into the rubbing surfaces easily. This stimulates to exploit MoS<sub>2</sub> nanosheets with an ultrathin structure as lubricating additives for DLC-based solid–liquid composite lubrication. As stated above, as compared to steel, DLC coating presents lower surface energy and higher chemical inertness [17–19]. Whether DLC coatings are able to react with MoS<sub>2</sub> nanosheets or play an inactive role remains mostly unknown. It is of importance to comprehend this so as to engineering valid DLC-based solid–liquid compound lubrication system.

In this work, the friction property of solid–liquid compound lubricating system with W-DLC coating was studied in the cases of lubricating by pure PAO oil and ultrathin MoS<sub>2</sub> nanosheets additivated oils. W-DLC was selected as the coating material because the W-DLC coating possess outstanding adhesion to substrate, low internal stress and excellent mechanical properties, and is one of the most promising films for industrial applications. In addition, the corresponding friction mechanism is discussed at the end.

## 2. Materials and Methods

### 2.1. Lubricants and Additives

Polyolefin oil (PAO 6, Shenzhen Huashengyuan Petroleum Technology Co., Ltd., Shenzhen, China) with the kinematic viscosity of 31.70 mm<sup>2</sup>/s at 40 °C and 5.95 mm<sup>2</sup>/s at 100 °C was used as the base oil. The MoS<sub>2</sub> nanosheets with an ultrathin structure applied in this paper were synthesized through a solvothermal approach, as explained in our previously published research [20].

### 2.2. Preparation and Characterization of W-DLC Coating

W-DLC film was deposited on the AISI 52,100 through the magnetron sputtering method. The W-DLC film was fabricated according to the published literature [21]. Samples in the shapes of balls and discs were applied as the substrates to deposit W-DLC coatings, respectively. The steel ball had a diameter of 10 mm, a surface roughness of 50 nm and a hardness of 61–63 HRC. The steel disc had a size of 24 mm in diameter and of 7.9 mm in thickness. Before deposition, the discs were ground and burnished to get a surface roughness of 50 nm. The thickness and cross-section image of the W-DLC film on the disc was detected through scanning electron microscopy (SEM, Thermo Fisher Scientific, Prague, Czech Republic). Prior to SEM observation, a small 5 × 5 × 7.9 piece was cut from the middle of the W-DLC coated disc by wire electrical discharge machining method. Its microhardness and elasticity modulus were tested by a nanoindentation tester (500-NHT3, Anton Paar, Boudry, Switzerland) with a diamond Berkovich (triangular pyramid) cusp, and the test parameters were a load of 10 mN and a hold of 30 s. The surface roughness of the coating was examined by an atomic force microscopy (AFM, Bruker, New York, NY, USA). The chemical component of the as-deposited film was gauged through X-ray photoelectron spectroscopy (XPS, Thermo Fisher Scientific, Prague, Czech Republic).

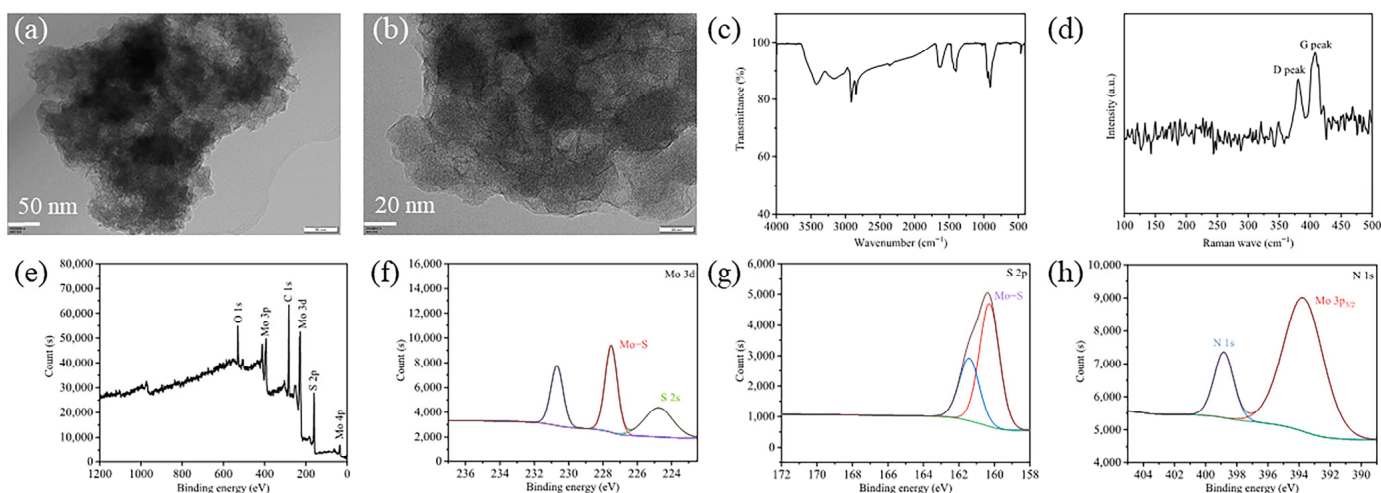
### 2.3. Friction Test

The friction tests were performed on a ball-on-disk tribotester (UMT-3, Bruker, New York, NY, USA). An oscillating frequency of 4 Hz and a stroke of 5 mm were utilized, giving a sliding velocity of 0.04 m/s. Each friction test lasted for 30 min and was iterated at least three times. During the friction, the ball was applied to slide against the W-DLC coated disc. Prior to experiments, fabricated MoS<sub>2</sub> nanosheets were dispersed into PAO 6 oil by ultrasonic agitation of 30 min. Then, the oil sample was dripped on the surface of the W-DLC coated disc with an amount of about 0.05 mL by a pipette, completely covering the rubbing surfaces. After friction tests, the disc was rinsed with acetone and the worn scar depth, and wear volume was observed through a white light interferometer (GT-X, Bruker, New York, NY, USA). The worn surface was also observed by SEM with energy-dispersive X-ray spectroscopy (EDS). XPS and Raman analyses were also used to characterize the worn surfaces.

## 3. Results and Discussion

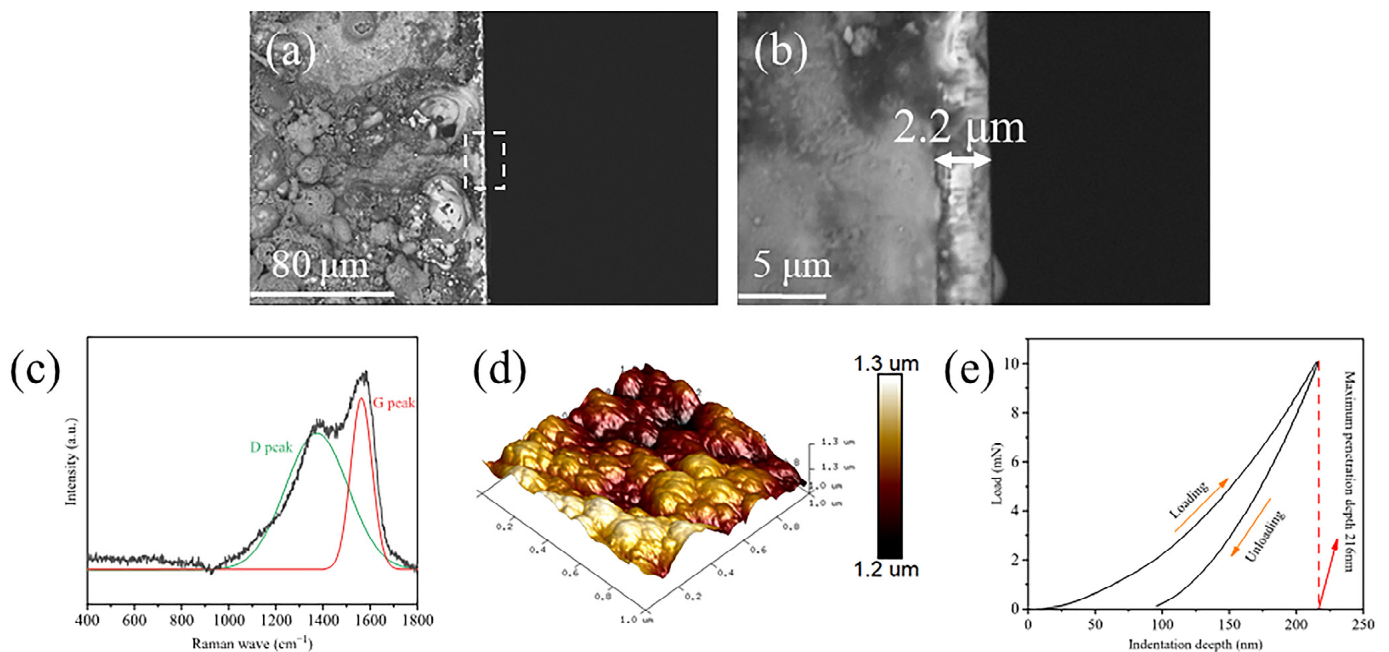
### 3.1. Structure and Morphology

Figure 1a,b present the TEM morphology of fabricated MoS<sub>2</sub> nanosheets, from which the ultrathin structure of MoS<sub>2</sub> nanosheets are observed. Meanwhile, the lateral size of the fabricated MoS<sub>2</sub> is around 30 nm. The FTIR spectrum of the prepared MoS<sub>2</sub> is illustrated in Figure 1c, in which the peaks at 2917, 2846, 1652, 1403 and 718 cm<sup>-1</sup> could be assigned to the bands belonging to oleylamine [16]. In addition, the peak at 470 cm<sup>-1</sup> can be assigned to the Mo-S bond [22,23]. This illustrates that the surfaces of synthesized MoS<sub>2</sub> nanosheets are attached by oleylamine molecules. Figure 1d is the Raman spectrum of the fabricated MoS<sub>2</sub>, in which the peaks at 381.5 and 405.3 cm<sup>-1</sup> belong to the E<sub>12g</sub> and A<sub>1g</sub> modes of MoS<sub>2</sub>, respectively [24,25]. Figure 1e–h shows the XPS analysis results of the prepared MoS<sub>2</sub>. As seen from Figure 1e, five elements of C, O, N, Mo, S are discovered, in which C and N are derived from oleylamine molecules, and O elements are attributed to pollutants adsorbed on the surface of MoS<sub>2</sub>. The two peaks in the Mo 3d spectrum at 227.52 and 230.68 eV could be distributed to Mo 3d<sub>5/2</sub> and Mo 3d<sub>3/2</sub> of Mo<sup>4+</sup> (Figure 1f). The S 2p spectrum has two peaks at 160.28 and 161.42 eV, which can point to S 2p<sub>3/2</sub> and S 2p<sub>1/2</sub> of S<sup>2-</sup> (Figure 1g). Meanwhile, the peak positions of Mo<sup>4+</sup> and S<sup>2-</sup> are very close to those reported values for MoS<sub>2</sub> [26,27]. In addition, the peak located at the position of 398.83 eV in the N 1s XPS spectrum can be attributed to N 1s (Figure 1h), which again confirms the decoration of oleylamine on the surfaces of MoS<sub>2</sub>.



**Figure 1.** (a,b) TEM image, (c) FTIR spectra, (d) Raman spectra, (e) XPS survey spectrum and high-resolution XPS spectra of (f) Mo 3d, (g) S 2p, (h) N 1s for the fabricated MoS<sub>2</sub>.

The cross-section of the W-DLC film on the steel disc is shown in Figure 2a,b. Obviously, the substrate surface is covered by a continuous layer of thin film. The thickness of the film is controlled at about 2.2  $\mu\text{m}$  (Figure 2b). The Raman spectrum of the deposited W-DLC film is shown in Figure 2c. Two strong peaks corresponding to the typical Raman peaks of DLC films are observed at  $1360\text{ cm}^{-1}$  (D band) and  $1560\text{ cm}^{-1}$  (G band). Figure 2d exhibits the AFM topography of the W-DLC coating. No sharp rough peaks are observed, and the surface roughness of the W-DLC film is approximately 8.15 nm. Figure 2e shows the nanoindentation curve of the W-DLC coating. Its hardness and elastic modulus were gauged at 12.48 GPa and 125.8 GPa, respectively. As shown in Figure 2e, when the test load is 10 mN, the maximum indentation depth is 216 nm, which is close to 10% of the W-DLC coating thickness (2.2  $\mu\text{m}$ ), and hence, the influence of the steel matrix on the mechanical characters of W-DLC coating is avoided.



**Figure 2.** (a,b) TEM images, (c) Raman spectrum, (d) AFM image, (e) nanoindentation load-displacement curve of W-DLC coating.

Furthermore, the chemical component of the W-DLC coating was tested through XPS. Figure 3a shows the full XPS spectrum, in which the C, O and W elements are detected, with the corresponding atomic percentage present in Table 1. It shows that the W-DLC film is composed of 84.34 at% of C, 15.56 at% of O and 0.1 at% of W, respectively. The O element may have been introduced during the preparation of the film, or it is possible that the W-DLC film is placed in the air before the experiment. The XPS spectra of C 1s and W 4f are revealed in Figure 3b,c. The C 1s spectrum can be decomposed into five peaks, namely, WC (283.31 eV),  $\text{W}_2\text{C}$  (283.81 eV),  $\text{sp}^2\text{-C}$  (284.6 eV),  $\text{sp}^3\text{-C}$  (285.41 eV) and C-O (286.57 eV) [28,29] (Figure 3b). The W 4f spectrum is shown in Figure 3c, and two states of W-C (at 33.61 and 35.69 eV) and W-O (at 34.64 and 37.15 eV) are found. As stated above, the oxygen element exists in the W-DLC coating as contaminants arising from external factors, and therefore, the W-O bond is observed.

**Table 1.** The XPS atomic percentage of W-DLC coatings.

Elements	C	O	W
Content, %	83.34	15.56	0.1

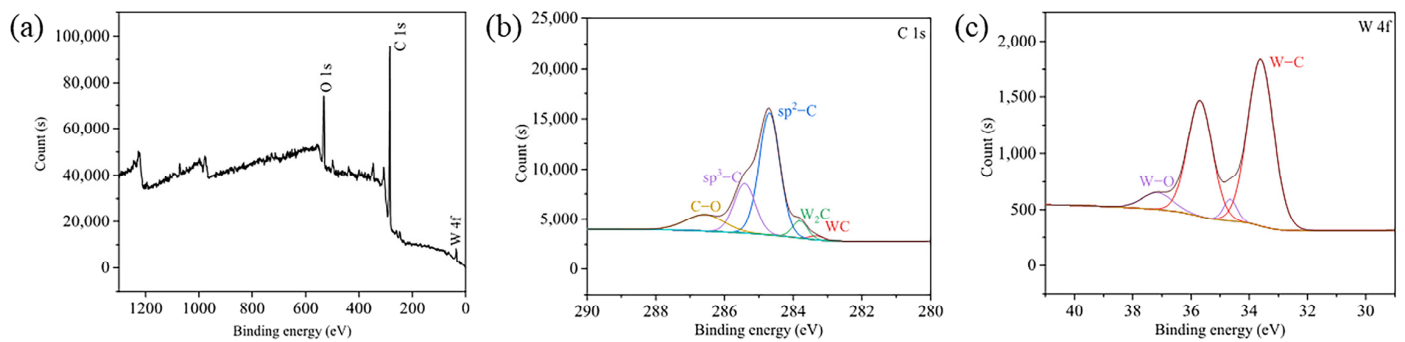


**Figure 3.** (a) XPS survey spectrum and high-resolution XPS spectra of (b) C 1s, (c) W 4f for W-DLC coating.

### 3.2. Tribological Property

Before friction tests, the dispersible stability of the lubricating oils additivated with MoS<sub>2</sub> nanosheets was examined by the precipitation observation method. The prepared MoS<sub>2</sub> were blended with the PAO oil at contents within a range of 1–5 wt%. Figure 4a shows the photographs of the oil samples after sitting for 3 h. Obviously, the appearance of the MoS<sub>2</sub>-containing oils stays black after standing 3 h. Furthermore, no significant precipitation is found at the sample bottoms (Figure 4b). This illustrates the good dispersion stability of synthesized MoS<sub>2</sub> nanosheets in the oils during the tribological tests.

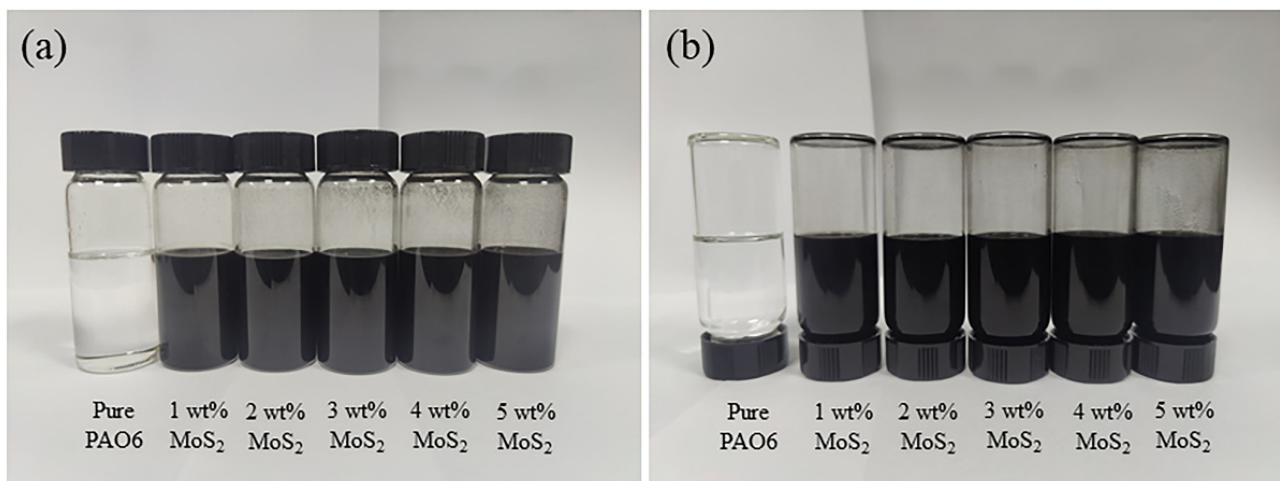


**Figure 4.** The photographs of oil samples after standing for 3 h with (a) sample bottles stood upright, (b) sample bottles upside down.

Figure 5 presents the tribological properties of steel/W-DLC and W-DLC/W-DLC tribopairs lubricated by the oils with different concentrations of fabricated MoS<sub>2</sub> (at the load of 20 N). As Figure 5a illustrated, the friction coefficient (COF) first increases and then decreases with increasing MoS<sub>2</sub> content in oils. A minimum COF value of 0.079 is obtained when the oil additivated with 4 wt% MoS<sub>2</sub>. At most, the COFs are reduced by 12.79% (steel/W-DLC contact) and 14.78% (W-DLC/W-DLC contact) in comparison with that lubricated by pure PAO oil. A promotion of the MoS<sub>2</sub> content from 4 wt% to 5 wt% could lead to an increase in the COF. This is attributed to the unavoidable agglomeration and accumulation at a high concentration of MoS<sub>2</sub> nanosheets, resulting in a damage of lubricant film. Figure 5b exhibits the worn scar diameters (WSDs) on the upper tribopairs with the changes of the MoS<sub>2</sub> nanoparticles' concentration. Obviously, the WSDs tend to be parabolic with the MoS<sub>2</sub> additives' concentration increasing, irrespective of pairs of friction materials. This could be explained by the fact that the oils with a low content of MoS<sub>2</sub> nanosheets could not offer a sufficient supply of lubricant additives in the late-stage of the

friction tests. On the contrary, the irreversible agglomeration and abrasive effects rising from the agglomeration of MoS<sub>2</sub> nanosheets at a high concentration greatly reduce the valid volume of lubrication constituents. For the steel/W-DLC couples, the WSDs are reduced by 3.08% and 0.84% after adding 3 wt% and 4 wt% into PAO oil, respectively, if compared to the pure PAO 6 oil. After adding 4 wt% MoS<sub>2</sub> nanosheets to PAO oil, the WSDs for the W-DLC/W-DLC tribopairs is reduced by 22.37%. As Figure 5 shows, the PAO oil with 4 wt% MoS<sub>2</sub> nanosheets exhibits a relatively better friction reduction and wear resistance properties, irrespective of tribopairs. Therefore, the MoS<sub>2</sub> nanosheets concentration in PAO 6 oil is fixed at 4 wt% for subsequent tribological tests.

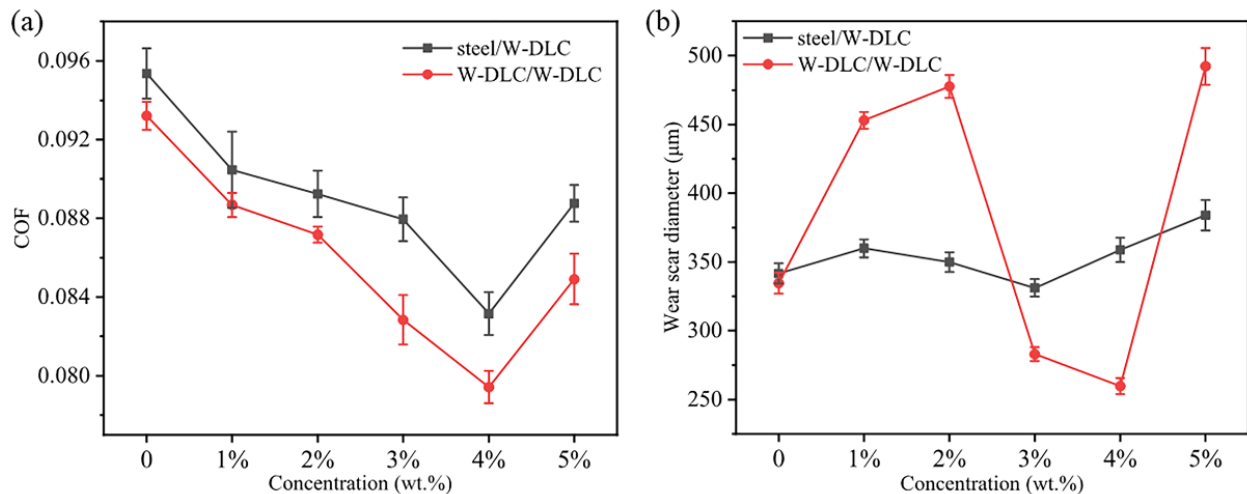
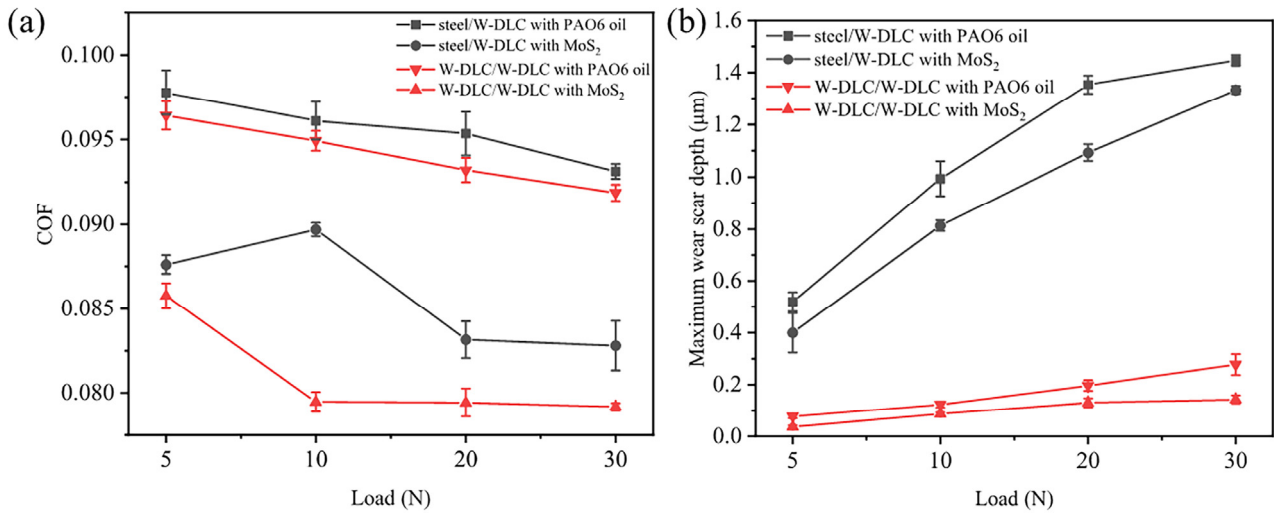


Figure 5. (a) COF and (b) wear scar diameter as functions of MoS<sub>2</sub> content in oils.

Figure 6 illustrates the influence of loads on the lubrication property of the steel/W-DLC and W-DLC/W-DLC contacts under different lubrication conditions. The experimental loads were set to 5 N, 10 N, 20 N and 30 N, respectively. As Figure 6a shows, there is not significant change in the COF as the function of the load. However, the MoS<sub>2</sub> additivated oil exhibits a relatively smaller COF than that of the pure PAO oil. In the steel/W-DLC couple, the average COF is calculated to be decreased by 10.83% after adding fabricated MoS<sub>2</sub> into the PAO oil. With regard to the W-DLC/W-DLC couple, the introduction of MoS<sub>2</sub> nanosheets into the PAO oil reduces the average COF by 15.44% compared to the pure PAO oil. Figure 6b illustrates the maximum wear scar depth of the lower W-DLC discs with the changes of applied load. Obviously, the maximum wear scar depth increases gradually with the changes of applied load, and there is a reduction in the maximum wear depth after adding fabricated MoS<sub>2</sub> into PAO oil. Moreover, it is clear from Figure 6b that the worn scar depth in the W-DLC/W-DLC couple is much shallower than that in the steel/W-DLC couple, irrespective of lubricating oils. For example, when tested with pure PAO oil, the average wear scar depth in the steel/W-DLC couple is 84.38% higher than that of W-DLC/W-DLC couple. As the MoS<sub>2</sub>-containing oils used for lubrication, the average wear scar depth is about 15.61% lower for the steel/W-DLC contact and this for the W-DLC/W-DLC contact is about 41.09%, compared with that lubricated by pure PAO oil. From Figure 6, it is evident that the lubricating effect of the MoS<sub>2</sub> in the W-DLC/W-DLC couple is more benefitting in comparison with the steel/W-DLC couple.

The worn scars of the rubbed W-DLC film were analyzed using the white light interferometer, which also allows for the wear volume of scars to be measured. Figure 7 shows a comparison between wear scars generated from the steel/W-DLC and W-DLC/W-DLC tribopairs. As expected, the wear volume of scratches deepens with increased applied load. As Figure 7a<sub>1</sub>–a<sub>4</sub> show, deep furrows are found on the worn surface generated from the steel/W-DLC contact lubricated by base PAO oil. For the W-DLC/W-DLC lubricated by PAO oil, the wear scar is relatively flat, and very slight scratches occur on the rubbing surfaces (Figure 7b<sub>1</sub>–b<sub>4</sub>). As the MoS<sub>2</sub>-added oil used for lubrication, the wear scars in

the steel/W-DLC couple turn much shallower in contrast to that lubricated by base PAO oil, and corresponding wear volumes are reduced significantly (Figure 7c<sub>1</sub>–c<sub>4</sub>). This result confirms the contribution of fabricated MoS<sub>2</sub> into improving the wear resistance property of PAO oil. However, no scratches are visible on the friction surface derived from W-DLC/W-DLC contact with an expectation at a high load of 30 N (Figure 7d<sub>1</sub>–d<sub>4</sub>).



**Figure 6.** (a) COF and (b) maximum wear scar depth under different loads.

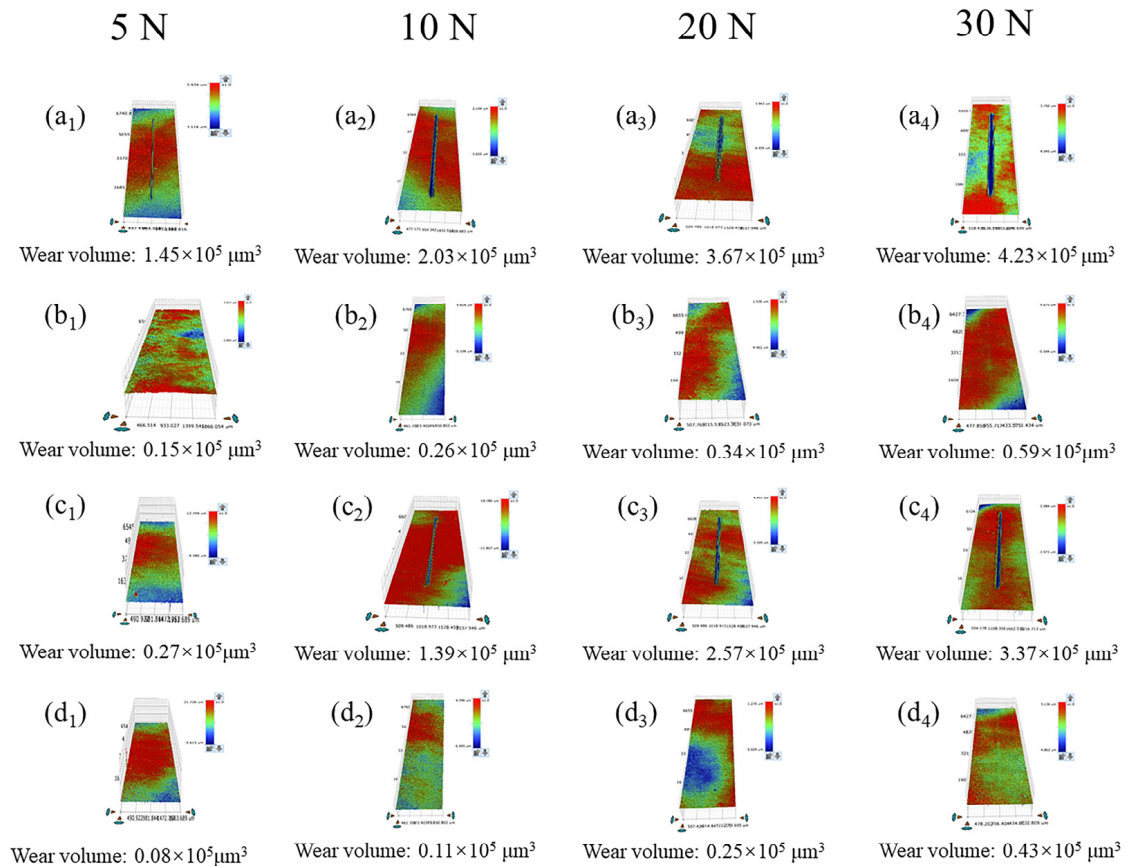


**Figure 7.** Three-dimensional images of the wear tracks derived from steel/W-DLC contact lubricated with (a<sub>1</sub>–a<sub>4</sub>) PAO oil or (c<sub>1</sub>–c<sub>4</sub>) MoS<sub>2</sub>-added oil and W-DLC/W-DLC contact lubricated with (b<sub>1</sub>–b<sub>4</sub>) PAO oil or (d<sub>1</sub>–d<sub>4</sub>) MoS<sub>2</sub>-added oil.

### 3.3. Wear Surface Analysis

The topographies of the above wear surfaces were investigated using SEM, with the results present in Figure 8. For the steel/W-DLC tribopairs, a lot of deep grooves are observed on the wear surface lubrication with pure PAO oil (Figure 8a<sub>1</sub>–a<sub>4</sub>), consistent with their 3D images, shown in Figure 7a<sub>1</sub>–a<sub>4</sub>. SEM images of worn surfaces for the W-DLC/W-DLC couple lubricated with pure PAO oil show relatively smooth wear surfaces only with some slight friction marks (Figure 8b<sub>1</sub>–b<sub>4</sub>). In the cases of the MoS<sub>2</sub>-containing oil for lubrication, the wear damage in the steel/W-DLC contact is significantly alleviated compared to that tested with pure PAO oil (Figure 8c<sub>1</sub>–c<sub>4</sub>). At the load of 5 and 10 N, the wear surfaces are covered a layer of tribofilm (Figure 8c<sub>1</sub>,c<sub>2</sub>). However, at a higher load of 20 N, it is found that a certain quantity of W-DLC coating is peeled off and delaminated from the steel substrate, as evident in Figure 8c<sub>3</sub>. When the imposed load increases to 30 N, the sign of grooves and plastic deformations are visible on the worn surface (Figure 8c<sub>4</sub>). As for the W-DLC/W-DLC tribopairs, the worn regions tested with prepared MoS<sub>2</sub> nanosheets exhibit quite smooth characteristics at 5 and 10 N, with the presence of a small amount of pits (Figure 8d<sub>1</sub>,d<sub>2</sub>). Comparatively, in the tests at 20 N and 30 N, the wear surfaces show quite smooth appearances without any evidence no sign of scratches (Figure 8d<sub>3</sub>,d<sub>4</sub>).

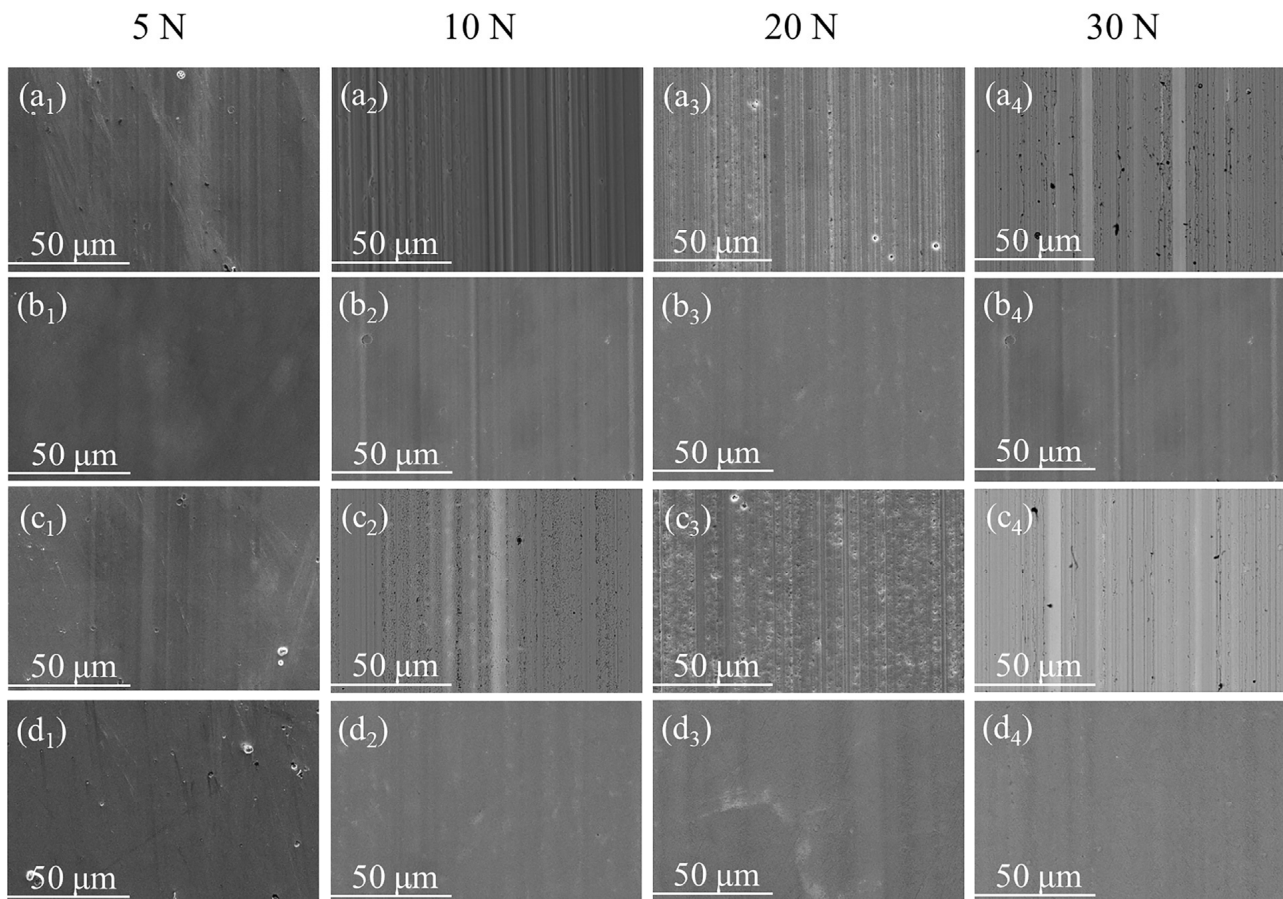


**Figure 8.** SEM images of the wear tracks from steel/W-DLC contact lubricated with (a<sub>1</sub>–a<sub>4</sub>) PAO oil or (c<sub>1</sub>–c<sub>4</sub>) MoS<sub>2</sub>-added oil and W-DLC/W-DLC contact lubricated with (b<sub>1</sub>–b<sub>4</sub>) PAO oil or (d<sub>1</sub>–d<sub>4</sub>) MoS<sub>2</sub>-added oil.

To analyze the elemental distribution of the worn marks on the W-DLC film coated discs tested in the presence of MoS<sub>2</sub> additives, EDS mapping was performed in the worn surfaces (Figure 8c<sub>3</sub>,d<sub>3</sub>), with the results shown in Figure 9. In both cases, the Mo and S elements appear on the worn scars. Prior to SEM analysis, the surfaces were ultrasonically cleaned with acetone, which guarantees that physically absorbed MoS<sub>2</sub> into rubbing sur-

faces can be removed. The remain of elements of Mo and S on worn surface, in spite of the ultrasonic cleaning, suggests a tribochemical reaction between the MoS<sub>2</sub> nanosheets and the W-DLC coating. Moreover, the worn scar derived from the W-DCL/W-DLC couple has more transferred Mo and S elements, indicates clearly the formation of a strong protective layer of MoS<sub>2</sub>-based tribofilm.

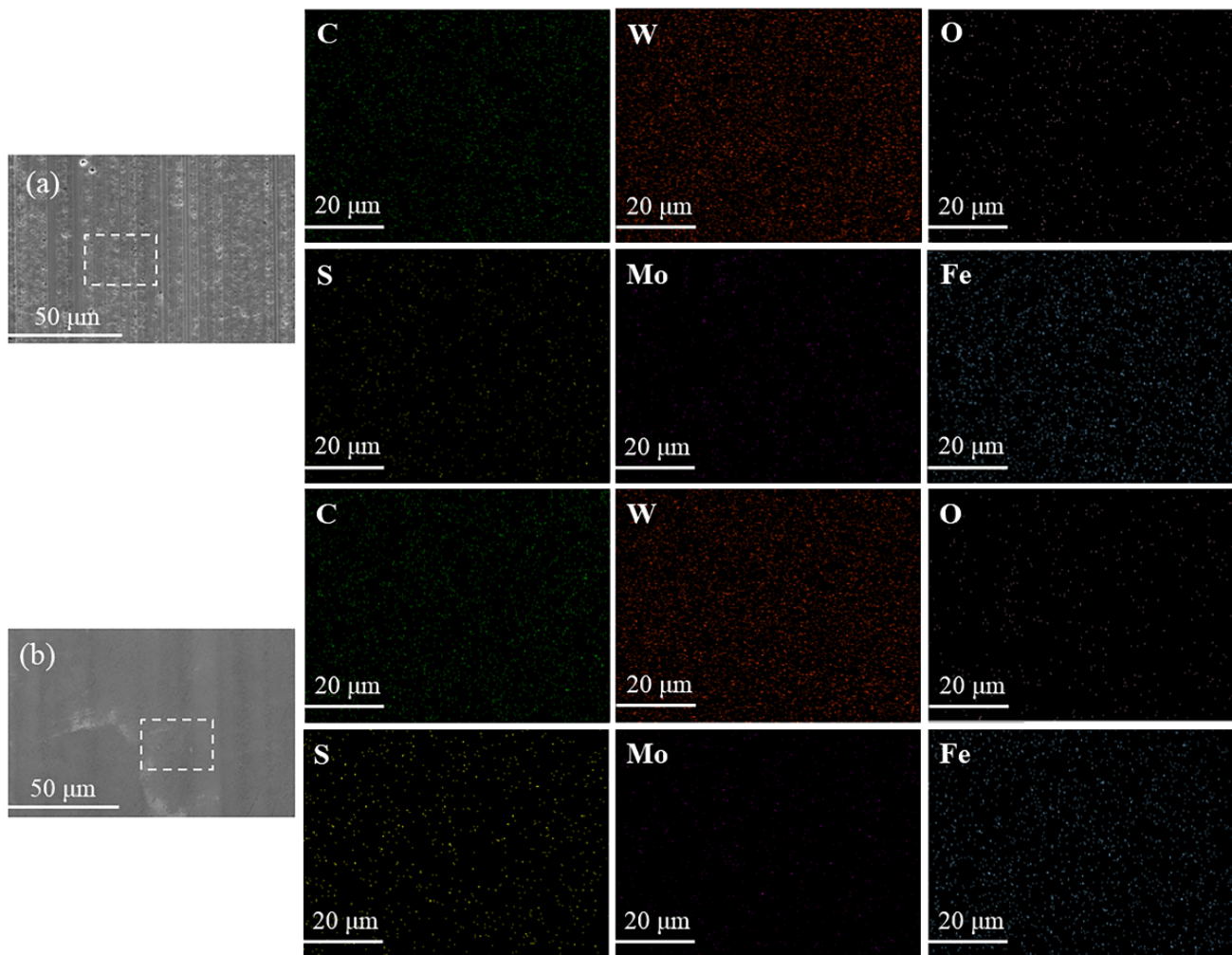


**Figure 9.** SEM images and the distribution of C, W, O, S, Mo and Fe elements on the wear tracks lubricated with MoS<sub>2</sub> from (a) steel/W-DLC contact and (b) W-DLC/W-DLC contact.

In order to further confirm whether the occurrence of interaction between the MoS<sub>2</sub> and the W-DLC coating, the worn scars on lower W-DLC specimens (Figure 8c<sub>2</sub>,d<sub>2</sub>) were examined by XPS analysis (Figure 10). Table 2 illustrates the quantification of XPS collected from the worn surface. The elements of C, W, O, Fe and Mo and S are discovered. The C, W and O elements could originate from the expected composition of their deposited coating. The minor Fe element could be derived from the steel substrate. Regardless of the type of tribopairs, Mo and S elements are found in the worn scars, which could be derived from the MoS<sub>2</sub> additives. In addition, a large concentration of O element, about 17–20 at%, is detected at the surfaces of W-DLC film, indicating that the W-DLC film was oxidized in the tribotest.

The XPS spectra of W 4f, C 1s, Mo 3d and S 2p were collected from two mentioned tribopairs (Figure 9a,b) and are displayed in Figure 11. As Figure 11 shows, the Mo 3d, C 1s, W 4f and S 2p XPS spectra for the two tribopairs tested with MoS<sub>2</sub> nano-additives are similar. The C 1s spectrum can be assigned into WC<sub>2</sub>, WC, sp<sup>2</sup>-C, sp<sup>3</sup>-C and C-O bonding states, respectively (Figure 11a<sub>1</sub>,b<sub>1</sub>). The W 4f spectrum exhibits six peaks, which correspond to

three tungsten-bonding states, i.e., W-C, WS<sub>2</sub> and WO<sub>3</sub>, respectively (Figure 11a<sub>2</sub>,b<sub>2</sub>). In contrast to the as-received W-DLC coating (Figure 3c), the W present in the rubbed W-DLC coating is transferred from WO<sub>2</sub> into the oxidized form of WO<sub>3</sub>. The Mo 3d<sub>5/2</sub> spectrum consists of the major peak belonging to MoS<sub>2</sub> and the minor peak arising from Mo-O (Figure 11a<sub>3</sub>,b<sub>3</sub>). As to the S 2p<sub>3/2</sub>, it consists of the S-W bond and MoS<sub>2</sub> (Figure 11a<sub>4</sub>,b<sub>4</sub>). The discovery of the S-W species in the Figure 11a<sub>4</sub>,b<sub>4</sub> indicates that the MoS<sub>2</sub> adhered onto the W-DLC coating via the bonding of W-S. Presumably, the generation of a tribofilm based on MoS<sub>2</sub> nanosheets is responsible for the worn resistance effect.

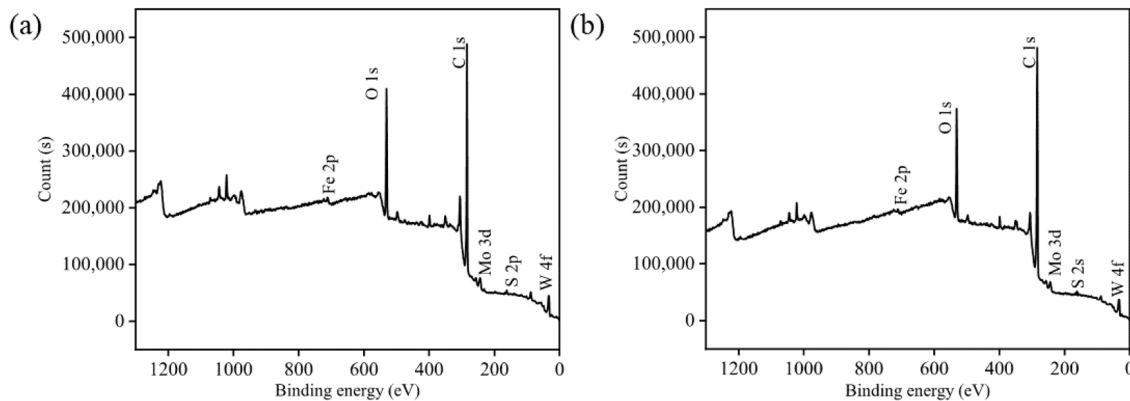


**Figure 10.** XPS survey spectra for the wear tracks lubricated with MoS<sub>2</sub> from (a) steel/W-DLC contact and (b) W-DLC/W-DLC contact.

**Table 2.** The XPS quantification for the steel/W-DLCW-DLC/W-DLC contacts.

Elements	C, %	O, %	W, %	S, %	Mo, %	Fe, %
steel/W-DLC	79.09	19.52	0.03	0.3	0.05	1.01
W-DLC/W-DLC	81.01	17.81	0.02	0.23	0.03	0.9

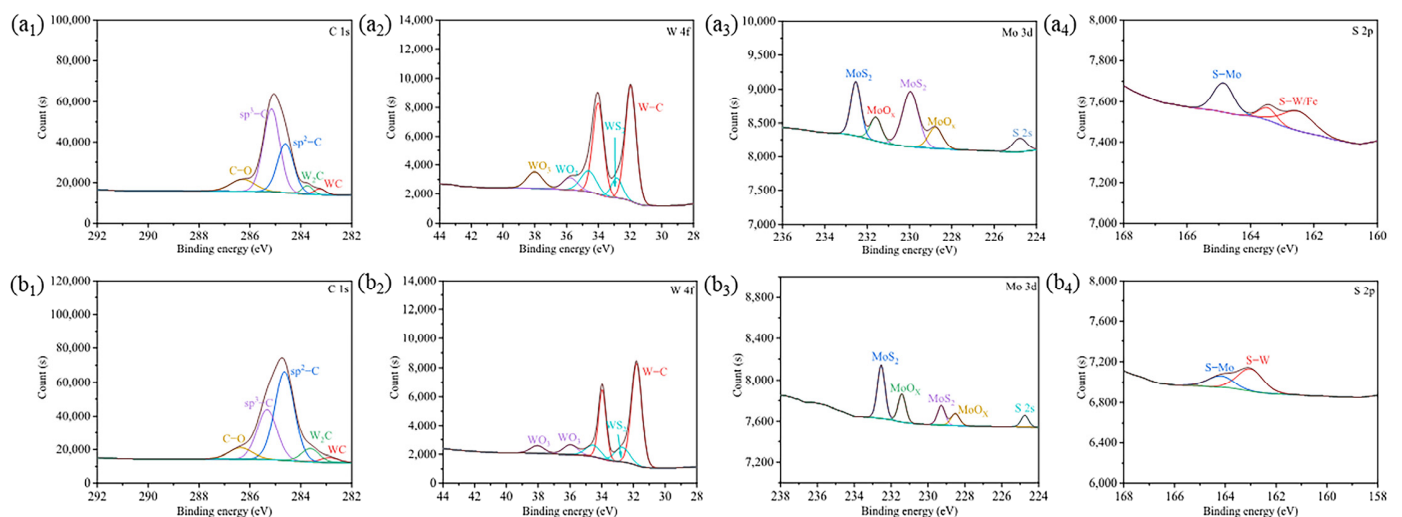


**Figure 11.** XPS spectra of C 1s, W 4f, Mo 3d and S 2p for wear tracks lubricated with MoS<sub>2</sub> from (a<sub>1</sub>–a<sub>4</sub>) steel/W-DLC and (b<sub>1</sub>–b<sub>4</sub>) W-DLC/W-DLC contact.

Furthermore, the wear marks on the W-DLC-coated discs (Figure 9a,b) were analyzed using Raman spectroscopy. As Figure 12 shows, the Raman spectra of the rubbed W-DLC coatings show a peak around 1360 cm<sup>-1</sup>, corresponding to the D band and a peak around 1560 cm<sup>-1</sup> attributed to the G band. However, the two rubbed surfaces exhibit a significant difference in the aspect of the peak ratio (I<sub>D</sub>/I<sub>G</sub>) of the D and G bands. It is well known that

the peak ratio ( $I_D/I_G$ ) value indicates the extent of graphitization of DLC coatings [30,31]. Moreover, the higher extent of graphitization is generally confirmed from the increase in the peak ratio ( $I_D/I_G$ ) of the D and G bands. Through curve fitting, the rubbed W-DLC coating generated from the steel/W-DLC contact present an  $I_D/I_G$  value of about 6.6, and this for the W-DLC/W-DLC contact is 0.82. Obviously, the peak ratio ( $I_D/I_G$ ) in the rubbed W-DLC coating from the steel/W-DLC couple is significantly higher than that for the W-DLC/W-DLC couple. This suggests that higher extent of graphitization occurred at the rubbed W-DLC surface generated from the steel/W-DLC couple as compared to the W-DLC/W-DLC couple. It is speculated that the microhardness of the W-DLC coating decrease arising from the increased extent of graphitization under applied loads, and therefore, induced the increase of wear rates of the W-DLC coating.

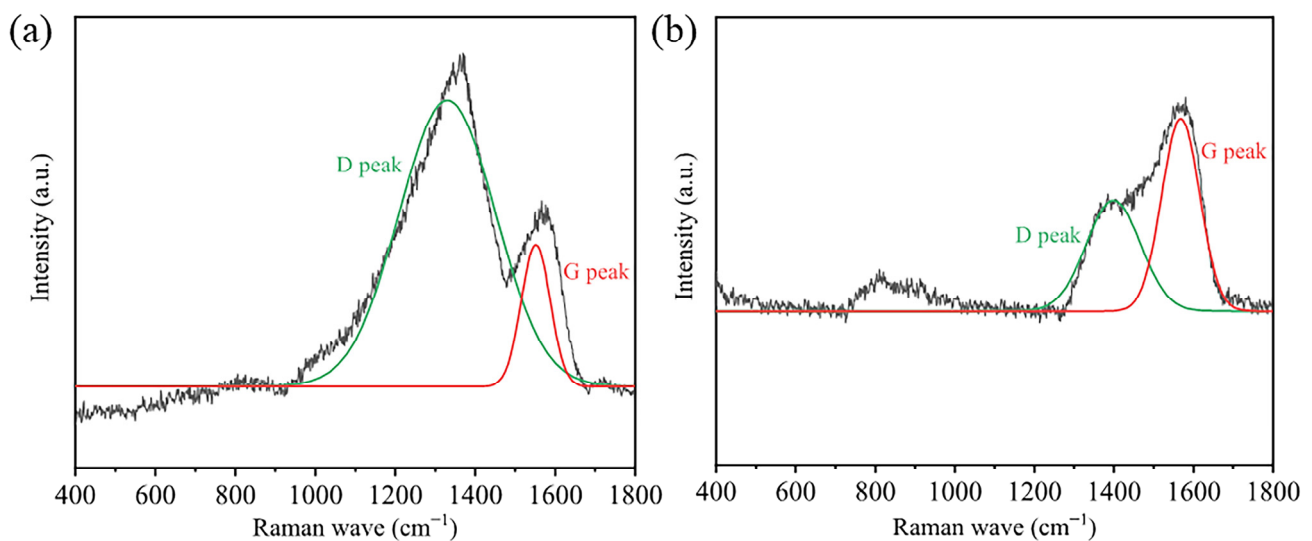


**Figure 12.** Raman spectra for the wear tracks lubricated with MoS<sub>2</sub> from (a) steel/W-DLC contact and (b) W-DLC/W-DLC contact.

Figure 13 illustrates the SEM images of the wear ball region derived from the steel/W-DLC and W-DLC/W-DLC tribopairs experimented with MoS<sub>2</sub> (at 20 N). It is obvious that compared to steel/W-DLC contact, the WSD of W-DLC/W-DLC is significantly reduced. For the steel/W-DLC contact (Figure 13a), there are a few debris particles scattered at the edge of the wear mark. Meanwhile, the Mo and S elements are mainly discovered at the margin, which may result from the broken MoS<sub>2</sub> nanosheets or their hard oxides. C and W elements are also observed on the worn ball surface. This can be interpreted as the W-DLC film being transferred to the ball when the naked ball slides on the W-DLC coated surface. With regard to the W-DLC/W-DLC couple (Figure 13b), some particle-like debris observed on the wear mark. Elements including C, W, O, Fe, Mo and S exist on the worn surface. In addition, there is an obvious distribution of Mo and S elements detected, indicating a continuous MoS<sub>2</sub>-based tribofilm on the worn surface.

### 3.4. Discussion

In this paper, the tribological behaviors of steel/W-DLC and W-DLC/W-DLC contacts were tested in the presence of base PAO 6 oil and ultrathin MoS<sub>2</sub>-containing oil. As seen from Figures 6 and 7, the friction is generally lower when two contact regions were coated with W-DLC than when only one counter-body was coated, which is observed in pure PAO oil and MoS<sub>2</sub>-additivated PAO oil.

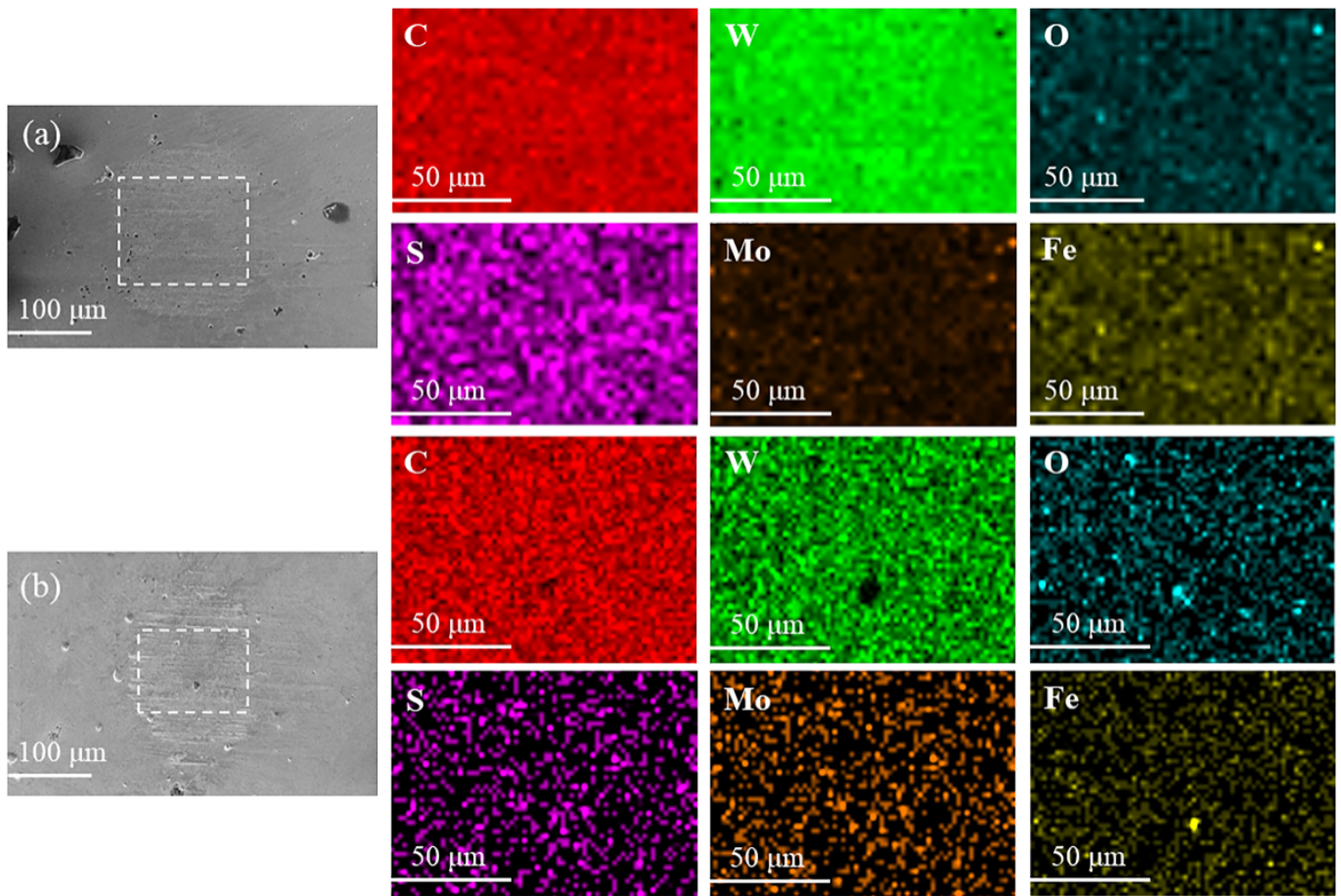


**Figure 13.** SEM images of the wear ball surfaces and the distribution of C, W, O, S, Mo and Fe elements, where tracks were lubricated with MoS<sub>2</sub> from (a) steel/W-DLC contact and (b) W-DLC/W-DLC contact.

As well known, the lubrication region of a ball–disc point contact pair can be determined by the film thickness ratio  $\lambda$  illustrated in Equation (1), which depends not only on the oil film ply, but also on the roughness of the frictional surfaces [32]:

$$\lambda = \frac{h}{\sqrt{R_{a1}^2 + R_{a2}^2}} \quad (1)$$

where  $R_{a1}$  and  $R_{a2}$  are the roughness of the two frictional surfaces, respectively, and  $h$  is the oil film thickness. When  $\lambda \leq 1$ , two frictional surfaces are lubricated at the boundary status; when  $1 < \lambda \leq 3$ , the mixed lubrication state occurred on two frictional pairs; when  $\lambda > 3$ , two frictional surfaces are absolutely separated with a lubricating film and stay in the fluid lubricant state.

The relevant oil film thickness ( $h_c$ ) in the central area can be calculated according to the Hamrock–Dowson formula [32]:

$$H_c^* = \frac{2.69G^{*0.53}U^{*0.67}(1 - 0.61e^{-0.73k})}{W^{*0.067}} \quad (2)$$

$$h_c = H_c^*R' \quad (3)$$

$$G^* = \alpha E', U^* = \frac{\eta_0 U}{E'R'}, W^* = \frac{W}{E'R'^2} \quad (4)$$

where  $h_c$  is the oil film plying in the central area,  $\alpha$  is the viscosity coefficient of the oil ( $3.5 \times 10^{-8} \text{ m}^2/\text{N}$ ),  $E'$  is the equivalent elasticity modulus (172.28 Gpa),  $U$  is the entrainment speed (0.02 m/s),  $\eta_0$  is the viscosity of the oil,  $R'$  is the equivalent radius,  $W$  is the applied load, and  $k$  is the ovality (1.03). According to the Equations (1)–(4), the results are present in Table 3, in which the  $\lambda$  value exhibits a value lower than 1, indicating that a boundary lubrication regime occurs during the friction process.

**Table 3.** Thickness of oil film under different loads.

Lubrication Conditions	Steel/W-DLC			W-DLC/W-DLC		
	10	20	30	10	20	30
Load, N						
Oil film thickness, nm	45.7	43.6	42.4	46.6	44.5	43.1
Composite roughness, nm	55.90	55.90	55.90	50.64	50.64	50.64
$\lambda_{initial}$	0.82	0.78	0.77	0.92	0.88	0.85

It is highly appreciated that an effective tribofilm exercise important influences on the friction behavior of oils in the boundary lubricating regime. Generally, it has been documented that the doping metal elements in DLC coating could provide reactive sites for the coating–lubricant interactions of forming a tribofilm [33]. Such behavior has been observed for the W-DLC coating in our paper, as confirmed by the XPS results shown in Figure 11. However, the friction could also induce the graphitization of W-DLC film, which resulted in local lamination of W-DLC films [34]. It is shown in Figure 13 that in contrast to the steel/W-DLC couple, the graphitization extent of W-DLC film in the self-mated W-DLC/W-DLC couple was significantly decreased. Two possible friction mechanisms are schematically presented in Figure 14. For the steel/W-DLC contact (Figure 14a), the pressure and temperature in the contact provoked the tribochemical reaction between  $\text{MoS}_2$  and the bare steel ball or the disc coated with W-DLC film forming a tribofilm separating two reciprocating surfaces. However, the W-DLC film was largely graphitized and oxidized under the friction conditions, resulting in the drop of its microhardness, and thus causing local delamination of W-DLC films. In addition, the carbon atoms in the DLC coating could be diffused into the ferrous surface because of the thermo-chemical interaction between the DLC coating and steel surface, which accelerated W-DLC coatings' wear [35]. Thus, the shift of W-DLC stuff from the lower W-DLC coated disc into the upper steel ball was observed in Figure 12a. In addition, the  $\text{MoS}_2$  nanosheets adhere onto the bare steel surface, and later, those nanoparticles slid against the W-DLC film, which could accelerate the wear of coated surface. As to the self-mated W-DLC/W-DLC couple, as shown in Figure 14b, a rather thick layers of tribofilm adheres to the DLC-coated surface through the tribochemical reaction between  $\text{MoS}_2$  and the W element doped in W-DLC, which has been demonstrated by an SEM observation in Figure 10. Furthermore, the tribofilm is formed at both counterparts, and they may keep the contacting asperities separated. In this case, the extent of graphitization of W-DLC film was alleviated because of the lubrication and protection from the  $\text{MoS}_2$ -based tribofilm on two friction surfaces, and a better lubrication effect was obtained.

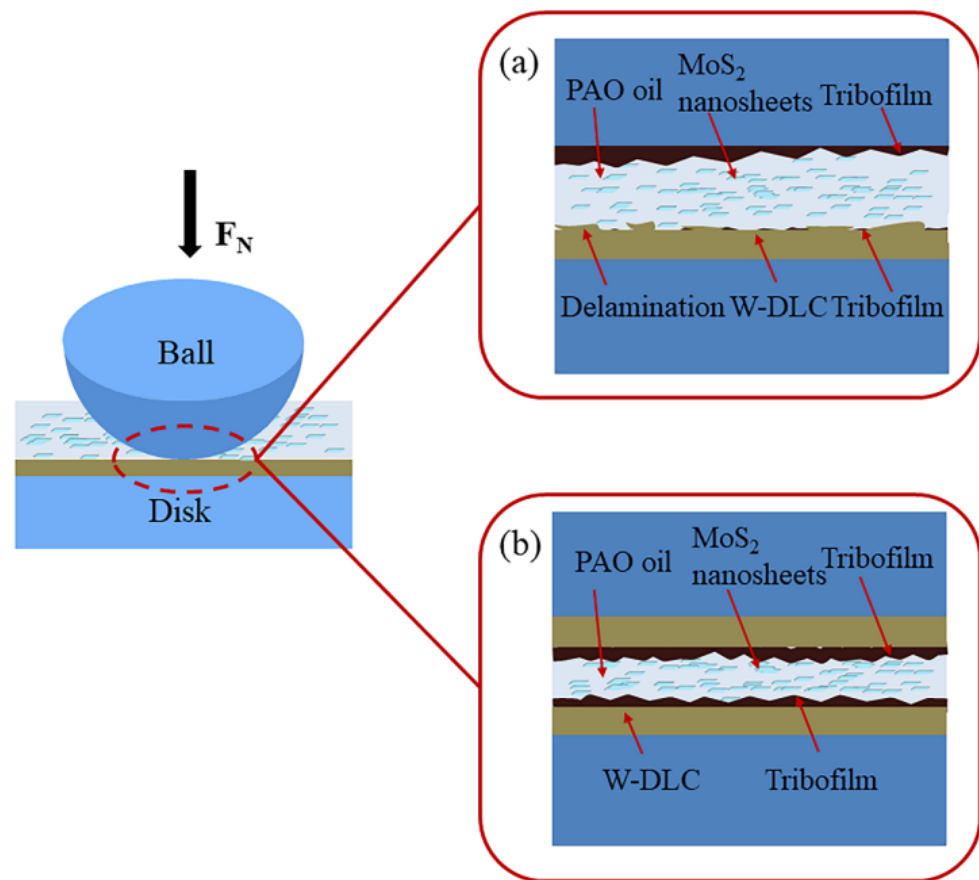


**Figure 14.** Schematic diagram of friction mechanisms for (a) steel/W-DLC and (b) W-DLC/W-DLC contact lubricated with MoS<sub>2</sub>.

#### 4. Conclusions

The friction property of the steel/W-DLC and W-DLC/W-DLC tribopairs were investigated under the boundary lubrication regime with MoS<sub>2</sub>-containing oil for lubrication. The introduction of ultrathin MoS<sub>2</sub> nanosheets into the PAO oil could importantly improve the friction behavior for the steel/W-DLC and W-DLC/W-DLC couples. And best results were gained for the W-DLC/W-DLC couple lubricated with ultrathin MoS<sub>2</sub> nanosheets, in which the friction coefficient and wear were decreased by 13.98% and 41.09% respectively, in comparison with the case of the W-DLC/W-DLC couple lubricated by pure PAO oil. Meanwhile, the reductions in the friction coefficient and wear were 4.98% and 89.10%, respectively, in contrast to the steel/W-DLC contact tested with ultrathin MoS<sub>2</sub> nanosheet additivated oils. The reason of friction reduction is the formation of MoS<sub>2</sub>-based friction film on rubbing regions. The tribofilm was formed by a tribochemical reaction between MoS<sub>2</sub> and the doping W elements in the DLC coating. Meanwhile, the extent of graphitization of W-DLC film was alleviated because of the lubrication and protection from the MoS<sub>2</sub>-based tribofilm. Wear marks were not obvious on the W-DLC/W-DLC couple, which suggested that combined with the good friction reduction and wear resistance behaviors of ultrathin MoS<sub>2</sub> additivated oil, the application of W-DLC coating prevented serious wear damage taking place. It can be deduced that an incorporation of W-DLC/W-DLC contact and MoS<sub>2</sub> nanosheets as oil additives provided an efficient solid–liquid composite lubricating effect.

**Author Contributions:** Conceptualization, Methodology, Investigation, Writing—review & editing, M.Y.; Writing—original draft, Investigation, T.W.; Data curation, Z.L.; Valition, J.L.; Valiation, J.Q.; Validation, Resources, W.X. All authors have read and agreed to the published version of the manuscript.

**Funding:** This research was financially supported by the National Natural Science Foundation of China (52065042), Natural Science Foundation of Jiangxi Province (20212BAB214059 and 20232BAB204040) and Tribology Science Fund of State Key Laboratory of Tribology (SKLTKF19B06).

**Data Availability Statement:** Data will be made available on request.

**Acknowledgments:** Specific thanks to School of Advanced Manufacturing and Key Laboratory of Tribology, Nanchang University for empowering the accomplishment of this study.

**Conflicts of Interest:** The authors declare no conflict of interest.

## References

1. Qi, J.; Wang, L.; Yan, F.; Xue, Q. The tribological performance of DLC-based coating under the solid-liquid lubrication system with sand-dust particles. *Wear* **2013**, *297*, 972–985.
2. Fan, X.; Xue, Q.; Wang, L. Carbon-based solid-liquid lubricating coatings for space applications: A review. *Friction* **2015**, *3*, 191–207.
3. Zhang, T.; Wan, Z.; Ding, J.; Zhang, S.; Wang, Q.; Kim, K. Microstructure and high-temperature tribological properties of Si-doped hydrogenated diamond-like carbon films. *Appl. Surf. Sci.* **2018**, *435*, 963–973.
4. Liu, Y.; Zhang, H. The synergistic mechanism between graphitized tribofilm and graphitized surface of diamond-like carbon film under different temperature environments. *Diam. Relat. Mater.* **2022**, *123*, 108875.
5. Liu, Y.; Zhang, H. Roles of transfer layer and surface adhesion on superlubricity behaviors of diamond-like carbon film depending on rotating and reciprocating motion. *Appl. Surf. Sci.* **2022**, *604*, 154538.
6. Tannous, J.; Dassenoy, F.; Lahouij, I.; Le Mogne, T.; Vacher, B.; Bruhacs, A.; Tremel, W. Understanding the tribochemical mechanisms of IF-MoS<sub>2</sub> nanoparticles under boundary lubrication. *Tribol Lett.* **2011**, *41*, 55–64.
7. Kalin, M.; Kogovsek, J.; Remskar, M. Nanoparticles as novel lubricating additives in a green, physically based lubrication technology for DLC coatings. *Wear* **2013**, *303*, 480–485.
8. Patel, J.; Kiani, A. Effects of reduced graphene oxide (rGO) at different concentrations on tribological properties of liquid base lubricants. *Lubricants* **2019**, *7*, 11.
9. Wang, J.; Zhang, H.; Hu, W.; Li, J. Modified Ni nanoparticles as additives in various greases: Assessment of comparative performance potential. *Lubricants* **2022**, *10*, 367.
10. Freschi, M.; Di Virgilio, M.; Zanardi, G.; Mariani, M.; Lecis, N.; Dotelli, G. Employment of micro- and nano-WS<sub>2</sub> Structures to enhance the tribological properties of copper matrix composites. *Lubricants* **2021**, *9*, 53.
11. Li, Z.; Chang, Q.; Meng, Y.; Yang, H.; Hao, L. In situ visualization study of tribofilm growth process from magnesium silicate hydroxide nanoparticles. *Tribol. Int.* **2023**, *187*, 108725.
12. Saffari, H.; Soltani, R.; Alaei, M.; Soleymani, M. Tribological properties of water-based drilling fluids with borate nanoparticles as lubricant additives. *J. Pet. Sci. Eng.* **2018**, *171*, 253–259. [[CrossRef](#)]
13. Yi, M.; Zhang, C. The synthesis of MoS<sub>2</sub> particles with different morphologies for tribological applications. *Tribol. Int.* **2017**, *116*, 285–294.
14. Chen, J.; Xu, Z.; Hu, Y.; Yi, M. PEG-assisted solvothermal synthesis of MoS<sub>2</sub> nanosheets with enhanced tribological property. *Lubr. Sci.* **2020**, *32*, 273–282. [[CrossRef](#)]
15. Chen, Z.; Liu, X.; Liu, Y.; Gunsell, S.; Luo, J. Ultrathin MoS<sub>2</sub> Nanosheets with Superior Extreme Pressure Property as Boundary Lubricants. *Sci. Rep.* **2015**, *5*, 12869.
16. Yi, M.; Qiu, J.; Xu, W. Tribological performance of ultrathin MoS<sub>2</sub> nanosheets in formulated engine oil and possible friction mechanism at elevated temperatures. *Tribol. Int.* **2022**, *167*, 107426. [[CrossRef](#)]
17. Zahid, R.; Masjuki, H.; Varman, M.; Mufti, R.; Kalam, M.; Gulzar, M. Effect of lubricant formulations on the tribological performance of self-mated doped DLC contacts: A review. *Tribol Lett.* **2015**, *58*, 32.
18. Shang, L.; Gou, C.; Li, W.; He, D.; Wang, S. Effect of microstructure and mechanical properties on the tribological and electrochemical performances of Si/DLC films under HCl corrosive environment. *Diam. Relat. Mater.* **2021**, *116*, 108385. [[CrossRef](#)]
19. Zhang, M.; Wu, G.; Lu, Z.; Shang, L.; Zhang, G. Corrosion and wear behaviors of Si-DLC films coated on inner surface of SS304 pipes by hollow cathode PECVD. *Surf. Topogr. Metrol. Prop.* **2018**, *6*, 034010. [[CrossRef](#)]
20. Yi, M.; Zhang, C. The synthesis of two-dimensional MoS<sub>2</sub> nanosheets with enhanced tribological properties as oil additives. *RSC Adv.* **2018**, *8*, 9564–9573. [[CrossRef](#)]
21. Li, D.; Kong, N.; Li, R.; Zhang, B.; Zhang, Y.; Wu, Z.; Zhang, Q. The tribological performance of W-DLC in solid-liquid lubrication system additivated with Cu nanoparticles. *Surf. Topogr. Metrol. Prop.* **2021**, *9*, 045043.
22. Rawat, S.; Harsha, A.; Agarwal, P.; Kumari, S.; Khatri, P. Pristine and alkylated MoS<sub>2</sub> nanosheets for enhancement of tribological performance of paraffin grease under boundary lubrication regime. *J. Tribol.* **2019**, *141*, 072102.
23. Chouhan, A.; Sarkar, K.; Kumari, S.; Vemuluri, S.; Khatri, P. Synergistic lubrication performance by incommensurately stacked ZnO-decorated reduced graphene oxide/MoS<sub>2</sub> heterostructure. *J. Colloid Inter. Sci.* **2020**, *580*, 730–739.
24. Kumari, S.; Chouhan, A.; Sharma, P.; Kuriakose, S.; Tawfik, A.; Spencer, S.; Walia, S.; Sugimura, H.; Khatri, P. Structural defects-mediated grafting of alkylamine on few-layer MoS<sub>2</sub> and its potential for enhancement of tribological properties. *ACS Appl. Mater. Inter.* **2020**, *12*, 30720–30730. [[CrossRef](#)] [[PubMed](#)]

25. Li, H.; Zhang, Q.; Yap, C.; Tay, B.; Edwin, T.; Olivier, A.; Baillargeat, D. From bulk to monolayer MoS<sub>2</sub>: Evolution of Raman scattering. *Adv. Funct. Mater.* **2012**, *22*, 1385–1390. [[CrossRef](#)]
26. Ma, C.; Qi, X.; Chen, B.; Bao, S.; Yin, Z.; Wu, X.; Luo, Z.; Wei, J.; Zhang, H.; Zhang, H. MoS<sub>2</sub> nanoflower-decorated reduced graphene oxide paper for high-performance hydrogen evolution reaction. *Nanoscale* **2014**, *6*, 5624–5629.
27. Wang, H.; Wang, B.; Wang, D.; Lu, L.; Wang, J.; Jiang, Q. Facile synthesis of hierarchical worm-like MoS<sub>2</sub> structures assembled with nanosheets as anode for lithium ion batteries. *RSC Adv.* **2015**, *5*, 58084–58090.
28. Gao, K.; Zhang, L.; Wang, J.; Zhang, B.; Zhang, J. Further improving the mechanical and tribological properties of low content Ti-doped DLC film by W incorporating. *Appl. Surf. Sci.* **2015**, *353*, 522–529.
29. Takeno, T.; Komiyama, T.; Miki, H.; Takagi, T.; Aoyama, T. XPS and TEM study of W-DLC/DLC double-layered film. *Thin Solid Film* **2009**, *517*, 5010–5013. [[CrossRef](#)]
30. Habibi, A.; Khoie, S.; Mahboubi, F.; Urgen, M. Raman spectroscopy of thin DLC film deposited by plasma electrolysis process. *Surf. Coat. Technol.* **2017**, *309*, 945–950.
31. Wong, P.; He, F.; Zhou, X. Interpretation of the hardness of worn DLC particles using micro-Raman spectroscopy. *Tribol. Int.* **2010**, *43*, 1806–1810. [[CrossRef](#)]
32. Wen, S.; Huang, P. *Principles of Tribology*; Tsinghua University Press: Beijing, China, 2012.
33. Miyake, S.; Saito, T.; Yasuda, Y.; Okamoto, Y.; Kano, M. Improvement of boundary lubrication properties of diamond-like carbon (DLC) films due to metal addition. *Tribol. Int.* **2004**, *37*, 751–761. [[CrossRef](#)]
34. Zhang, Y.; Zhang, S.; Sun, D.; Yang, G.; Gao, C.; Zhou, C.; Zhang, C.; Zhang, P. Wide adaptability of Cu nano-additives to the hardness and composition of DLC coatings in DLC /PAO solid-liquid composite lubricating system. *Tribol. Int.* **2019**, *138*, 184–195. [[CrossRef](#)]
35. Mannan, A.; Sabri, M.; Kalam, M.; Hassan, M. Tribological performance of DLC/DLC and steel/DLC contacts in the presence of additivated oil. *Int. J. Surf. Sci. Eng.* **2018**, *12*, 60–75. [[CrossRef](#)]

**Disclaimer/Publisher's Note:** The statements, opinions and data contained in all publications are solely those of the individual author(s) and contributor(s) and not of MDPI and/or the editor(s). MDPI and/or the editor(s) disclaim responsibility for any injury to people or property resulting from any ideas, methods, instructions or products referred to in the content.